Research Article

The Morphostructural, Compositional, and Electrochemical Characterization of Electrodeposited Nanolayers on a New Ti-15Ta-5Zr Alloy

Cora Vasilescu, Silviu Iulian Drob, Petre Osiceanu, Mihai Anastasescu, Jose M. Calderon-Moreno, Paula Drob, and Ecaterina Vasilescu

Romanian Academy, Institute of Physical Chemistry "Ilie Murgulescu", Splaiul Independentei 202, 060021 Bucharest, Romania

Correspondence should be addressed to Silviu Iulian Drob; sidrob@chimfiz.icf.ro

A porous, homogeneous, phosphorous-enriched oxide nanolayer was realized on the new Ti-15Ta-5Zr alloy surface by the anodic galvanostatic electrodeposition in phosphoric acid solution. This nanolayer contains TiO_2, ZrO_2 oxides, tantalum suboxides, and PO_4^{3-} ions incorporated in the time of the electrodeposition process and has a thickness of 15.5 nm (X-ray photoelectron spectroscopy data). Atomic force microscopy determined a homogeneous roughness. Scanning electron microscopy evinced a porous microstructure that can stimulate the growth of the bone tissue into pores. The presence of the PO_4^{3-} anions promotes the electrostatic bonds between the nanolayer and different species from the biofluid, namely, osteoinduction. The anodic oxidation nanolayer improved all electrochemical and corrosion parameters conferring superior protection to the substrate by its higher resistance to the ion migration. Impedance spectra showed that the electrodeposited nanolayer is formed by an inner, dense, barrier layer and an outer porous layer. The nanolayer thickened in time, namely, is bioactive. The oxidized nanolayer is able to protect the alloy from ion release, to assure long-term corrosion resistance, to minimize adverse reactions, to increase alloy bioactivity, to stimulate cell growth, and to favor osseointegration.

1. Introduction

Titanium and its alloys represent a class of materials with large applications both in industry (aerospace, marine, and chemical) and medicine due to their very high corrosion resistance. In medicine, Ti and its alloys used to bone reconstructions have accomplished numerous criteria for dental and orthopedic implants: biocompatibility [1], nonallergic reactions, inertness to the human body fluids, rigidity, low density and elasticity (closed to the bone) [2], good mechanical properties, wear and fatigue resistance, bone bonding ability, and so forth, [3, 4]. The anticorrosive resistance is the most decisive property for the biocompatibility of metallic materials because it reduces very much the ion release into the biofluid; Ti and its alloys realize this need as result of the existence of a very stable oxide, passive film on their surfaces, but this film can be altered by the bone movement that can produce wear corrosion [5]. A method to avoid these shortcomings is the thickening of this passive film by different

techniques. In the same time, it is necessary to assure the very good attachment of the bone cells with the metallic implant by the modification of the surface topography, roughness, and so on, to increase the binding and fixation between them.

An efficient, cheap, easy method to thicken the protective oxide films is the electrochemical anodization. This method is more convenient than other methods as plasma spray, sol-gel, chemical or physical vapor deposition, ion implantation, and so forth, because, in addition, the adherence of the formed oxide layer is very high, and its thickness can be controlled by the electrodeposition parameters, can be applied on the complex surfaces, can incorporate ions (as phosphates) and species from the deposition solutions which can reinforce its protective capacity, and can promote the formation of phosphate, the main inorganic component of the bone, therefore the bioactivity of the metallic implant, and implicitly its direct contact with the bone. The electrochemical anodization can be performed by potentiostatic and

galvanostatic polarization. The potentiostatic anodization [6–14] uses expensive equipment, potentiostat, and under a high anodic voltage, in different acidic or neutral solution, the oxide layer grows. The galvanostatic anodization [4, 5, 15–19] produces by a versatile way a uniform, relative high porous, rough oxide layer that contains ions, and elements from the electrodeposition solution.

We obtained a porous, homogeneous nanolayer on the new Ti-15Ta-5Zr alloy surface by the anodic galvanostatic electrodeposition in phosphoric acid H_3PO_4 solution; varying different parameters as solution concentration, current density, deposition time, the most favorable nanolayer with the best rough (by Atomic Force Microscopy (AFM)), morphology (by Scanning Electron Microscopy (SEM)), and composition and thickness (by X-ray Photoelectron Spectroscopy (XPS)) was selected and its electrochemical behavior and corrosion resistance in Ringer physiological solutions of different pH values, simulating the real functional conditions of an implant, were determined by the potentiodynamic cyclic and linear polarization and electrochemical impedance spectroscopy (EIS). Also, the long-term behavior of the obtained nanolayer was studied from the monitoring of the open circuit potentials and corresponding open circuit potential gradients in Ringer solutions.

2. Experimental Details

The new Ti-15Ta-5Zr alloy was synthesized by two successive vacuum melting in semilevitation furnace with cold crucible. The raw materials had high purity and the composition of the as-cast ingots was (%wt.): 0.011% H; 0.02% N; 0.12% O; 0.015% Si; 0.0074% Zn; 0.0035% Nb; 0.0052% Sn; 14.26% Ta; 4.771% Zr; balance Ti.

2.1. Electrodeposition of the Nanolayers. Before the electrodeposition, the cylindrical electrodes were progressively ground with emery paper (from 400 till 2000 mesh) and mirror-polished with aluminum paste. Then, the samples were ultrasonically degreased in acetone and water for every 15 min and dried in air. The anodic galvanostatic electrodeposition was applied by a high power current source (Matrix, China) in H_3PO_4 solutions of different concentrations, 0.5 M–1.5 M, at anodic current densities varying between $5 \, mA/cm^2$ and $15 \, mA/cm^2$, for various time periods from 15 min till 90 min. Optical observations showed that at low acid concentration, current density, and time, the obtained nanolayer did not covered the entire surface. In proportion as the values of these three electrodeposition parameters (concentration, current density, and time) increased, the colored thin layers from gold to blue could be observed; these nanolayers were characterized by different techniques and the nanolayer with the most favorable microstructural properties was selected.

2.2. Characterization of the Electrodeposited Nanolayers. The composition and thickness of the electrodeposited nanolayer were analyzed by X-ray Photoelectron Spectroscopy (XPS), its topography and roughness by Atomic Force Microscopy (AFM), and its microstructure, morphology, and porosity by Scanning Electron Microscopy (SEM).

2.2.1. X-Ray Photoelectron Spectroscopy. XPS was applied by Quantera SXM equipment at a pressure of 1.33×10^{-7} Pa; the X-ray source was AlK_α radiation (1486.6 eV monochromatized) by a full width at half maximum (FWHM) of $Au4f_{7/2}$ line. The spectra were calibrated with C 1s line (binding energy BE = 284.8 eV) of the adsorbed hydrocarbon on the sample surface. A dual beam neutralizing procedure (e^- and Ar^+ ion beams) has been used to compensate the charging effect in the insulating samples. The errors in the quantitative analysis were estimated in the range of ±10%, and the accuracy for the BEs was ±0.2 eV. The thickness of the electrodeposited layer was determined by XPS depth profiling, layer by layer experiment under 1 keV and 3×3 mm scanning area, 45° incident angle, and 100 μm spot size. These parameters were used to minimize the reduction effect of the ion beam on the surface oxides.

2.2.2. Atomic Force Microscopy. AFM measurements were carried out in the noncontact mode with XE-100 apparatus equipped with flexure-grinded, cross-talked eliminated scanners, using sharp tips (radius < 7 nm) of about 225 μm length, 38 μm width, and 48 N/m spring constant at ca. 190 kHz resonance frequency. The topographical 2D and 3D AFM images were taken over an area of 2×2 μm and were used to calculate root mean square (RMS) and average surface (Rav) roughness.

2.2.3. Scanning Electron Microscopy. SEM micrographs were obtained with FEI Quanta 2DFEG Dual Beam system operating in secondary (SE) and back-scattered (BSE) detector at an accelerating voltage of 5 kV.

2.3. Electrochemical Methods. Electrochemical and corrosion behavior of the most favorable electrodeposited nanolayer were examined by cyclic potentiodynamic and linear polarization and electrochemical impedance spectroscopy (EIS) [20–26].

Cyclic potentiodynamic polarization furnished the cyclic voltammograms and the main electrochemical parameters: corrosion potential, E_{corr}; passivation potential, E_p; tendency to passivation, $|E_{corr} - E_p|$; passive potential range, ΔE_p; passive current density, i_p. The cyclic potentiodynamic polarization curves were registered from about −800 mV till +2000 mV (versus SCE) with a scan rate of 1 mv/s, using Voltalab 80 equipment.

Potentiodynamic linear polarization was performed for ±50 mV around the open circuit potential at a scan rate of 0.5 mV/s using the same Voltalab 80 equipment. VoltaMaster 4 program adjusted Tafel curves and directly supplied the values of corrosion current density, i_{corr}; corrosion rate, V_{corr}; polarization resistance, R_p; the total quantity of ions released into solution was calculated [27].

EIS was applied at the open circuit potential with 5 mV voltage amplitude in the frequency range from 10^{-1} Hz to 10^5 Hz with 7 points per decade. The Voltalab 80 equipment

and its VoltaMaster 4 program displayed Nyquist and Bode spectra. Zview program modeled the electric equivalent circuit.

The electrochemical behavior of the electrodeposited nanolayer on the Ti-15Ta-5Zr alloy surface in comparison with base alloy was studied in Ringer physiological solutions of different pH values (acid pH = 3.54, obtained by HCl addition; neutral pH = 7.49; alkaline pH = 8.98, obtained by KOH addition), simulating the real functional conditions of an implant. In case of surgery, the local acidification of the biofluid can appear due to the traumatisms [28]. In the distress periods of the human body (infections or inflammations), local alkalinity can form [29].

Ringer solution composition was (g/L): NaCl—6.8; KCl—0.4; $CaCl_2$—0.2; $MgSO_4 \cdot 7H_2O$—0.2048; $NaH_2PO_4 \cdot H_2O$—0.1438; $NaHCO_3$—1.1; glucose—1. Temperature was kept at $37° \pm 1°C$.

The open circuit potentials E_{oc} of the bare and oxidized Ti-15Ta-5Zr alloy were monitored for 500 immersion hours in Ringer solutions using a performing Hewlett-Packard multimeter.

The open circuit potential gradients ΔE_{oc} [27] which can develop along the implant surface due to the local nonuniformity of the physiological solution pH were calculated as:

$$\Delta E_{oc1}\left(\text{pH}\right) = E_{oc}^{\text{pH}=3.54} - E_{oc}^{\text{pH}=7.49},$$

$$\Delta E_{oc2}\left(\text{pH}\right) = E_{oc}^{\text{pH}=3.54} - E_{oc}^{\text{pH}=8.98}, \qquad (1)$$

$$\Delta E_{oc3}\left(\text{pH}\right) = E_{oc}^{\text{pH}=7.49} - E_{oc}^{\text{pH}=8.98}.$$

3. Results and Discussion

3.1. Composition and Thickness of the Electrodeposited Nanolayer. XPS analysis showed that the nanolayer obtained by the electrodeposition in 1.1 M H_3PO_4 solution at a current density of 12 mA/cm^2 for a period of 50 min had the most convenient composition, thickness and price. XPS survey spectrum (Figure 1) identified the main peaks of binding energies for Ti 2p, Ta 4f, Zr 3d (the constituent elements of Ti-15Ta-5Zr alloy), and, in addition, O 1s and P 2p [30, 31] incorporated from the electrolyte.

High resolution XPS spectra (Figure 2) for the nanolayer electrodeposited at 12 mA/cm^2, in 1.1 M H_3PO_4 solution for 50 min indicated that the doublet of Ti 2p (Figure 2(a)) had a peak at a binding energy of 458.8 eV that is specifically for TiO_2 protective oxide [30–33]; the doublet of P 2p (Figure 2(d)) contains a peak at 133.8 eV representing $PO_4{}^{3-}$ ion [33, 34] incorporated from solution; O 1s spectrum (Figure 2(e)) is formed by peaks for O^{2-} ion and adsorbed H_2O and OH^- ion; the peak of OH^- ion at a binding energy of 531.8 eV [33, 34] shows the existence of oxygen from $PO_4{}^{3-}$ ion; the peak of O^{2-} ion at 529.5 eV [35, 36] confirms the formation of oxides; additionally, Ta 4f spectrum (Figure 2(b)) denotes the peaks for tantalum suboxides [30, 31] (Ta_2O, TaO, and TaO_2) at about 26 eV and 28 eV; also, the doublet of Zr 3d (Figure 2(c)) clearly ascertains the ZrO_2 oxide [30, 31] at about 182 eV. It results that, by the anodic galvanostatic polarization at 12 mA/cm^2, for 50 min

TABLE 1: Roughness of Ti-15Ta-5Zr alloy surface after anodic galvanostatic polarization.

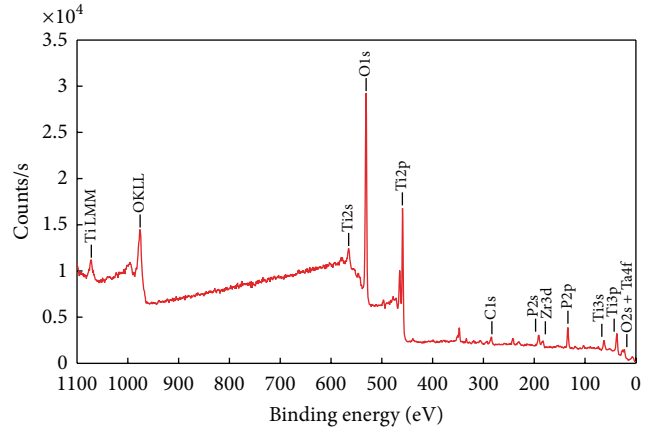| Electrodeposition conditions	RMS (nm)	Rav (nm)
0.5 M H_3PO_4, 10 mA/cm^2, 45 min	10.52	8.73
1.1 M H_3PO_4, 12 mA/cm^2, 50 min	55.83	40.67

FIGURE 1: XPS survey spectrum for the nanolayer electrodeposited at 12 mA/cm^2, in 1.1 M H_3PO_4 solution for 50 min.

in 1.1 M H_3PO_4 solution, the surface of Ti-15Ta-5Zr alloy was covered with a nanolayer formed by TiO_2, ZrO_2, oxides, tantalum suboxides, and $PO_4{}^{3-}$ ions incorporated in the time of the electrodeposition process. The presence of $PO_4{}^{3-}$ ions is very beneficial because these ions being the main inorganic component of the human bone will promote the ulterior codeposition of phosphate ions and will react with ions from the physiological fluid, which means bioactivity [2] and biocompatibility.

The thickness of the layer existing on the Ti-15Ta-5Zr alloy surface after anodic galvanostatic polarization at 12 mA/cm^2 for 50 min in 1.1 M H_3PO_4 solution was calculated from XPS depth profiling spectra as being 15.5 nm ± 1.0 nm [37]; comparing with the thickness of 8.5 nm ± 1 nm of the native passive film (unshown results), it appears that by the electrodeposition, the new layer doubled its thickness.

3.2. Topography and Roughness of the Electrodeposited Nanolayer. The topography and roughness play an important role for the interfacial reactions between the implant and local tissues [6]. AFM 3D images (Figure 3) revealed that in 0.5 M H_3PO_4 solution at a current density of 10 mA/cm^2 for 45 min was electrodeposited a nanolayer with nonporous topography (Figure 3(a)), while in 1.1 M H_3PO_4 solution at a current density of 12 mA/cm^2 for 50 min, it resulted in a rough nanolayer with homogeneous roughness and porosity (Figure 3(b)). Table 1 evinced the differences between the roughness of these two electrodeposited nanolayers; namely, both RMS and Rav have five times higher values for the nanolayer obtained in 1.1 M H_3PO_4 solution at a current density of 12 mA/cm^2 for 50 min.
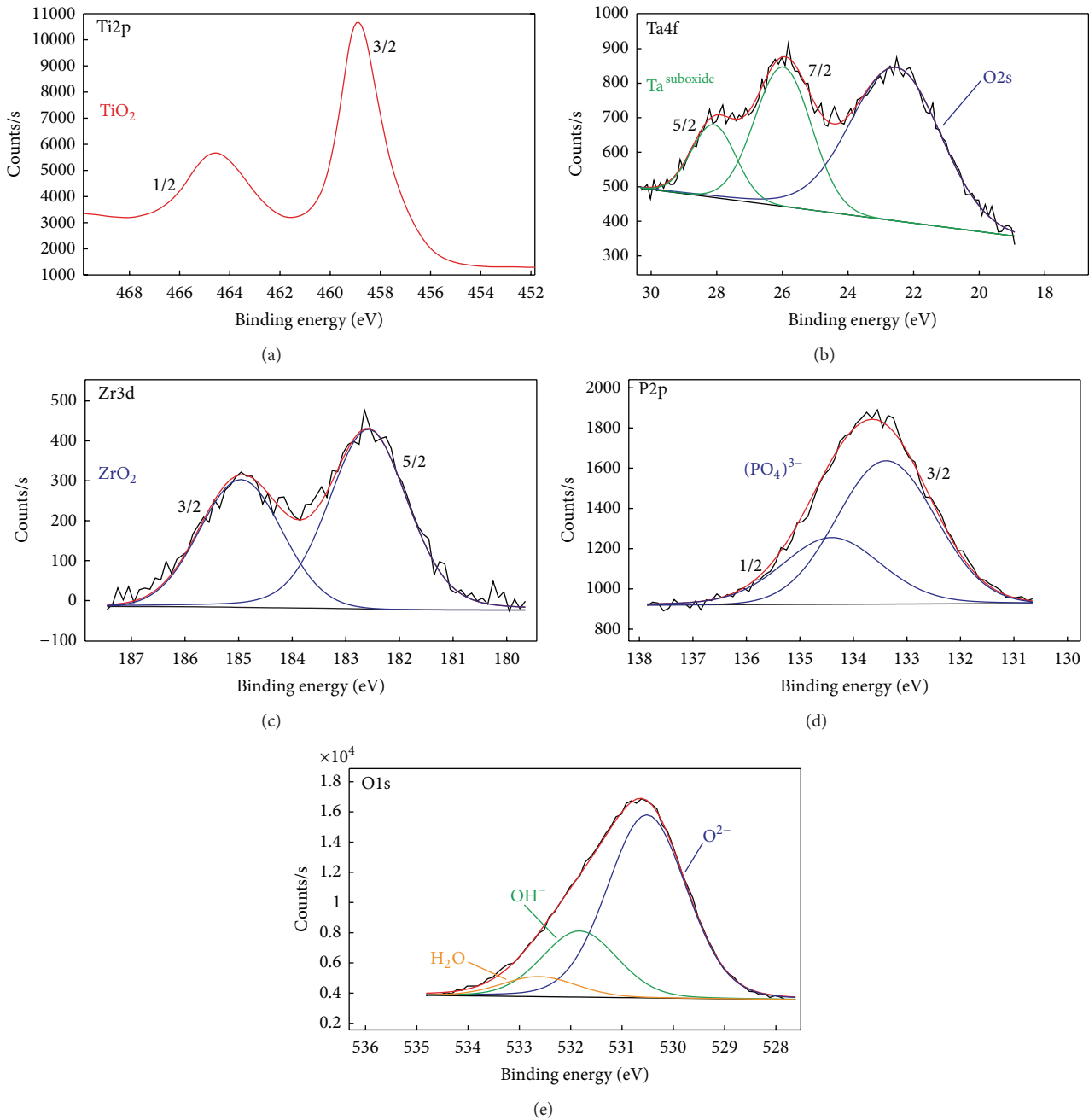
(a)

(b)

(c)

(d)

(e)

FIGURE 2: XPS high resolution spectra for the nanolayer electrodeposited at $12 \, mA/cm^2$, in $1.1 \, M \, H_3PO_4$ solution for 50 min: (a) Ti 2p; (b) Ta 4f; (c) Zr 3d; (d) P 2p; (e) O 1s.

This roughness and the presence of PO_4^{3-} anions on the Ti-15Ta-5Zr alloy surface favor the migration of the different ions into the pores of the nanolayer and reactions of ion exchange with the ions from the human body fluid; namely, the surface has polyanionic properties [6]; these facts promote the electrostatic bonds between electrodeposited nanolayer and proteins, fibronectin, fibroin, osteocalcin, and osteoblast, that is, biomineralization of this rough surface that so induces the growth of the bone tissue into pores and consequently a strong mechanical interlocking between implant surface and bone tissues [6]. Therefore, the nanolayer

electrodeposited in $1.1 \, M \, H_3PO_4$ solution at a current density of $12 \, mA/cm^2$ for 50 min, containing protective TiO_2, ZrO_2 oxides, tantalum suboxides, and PO_4^{3-} anions, has osteoinductive properties and develops a strong bone adhesion.

3.3. Morphology and Porosity of the Electrodeposited Nanolayer. SEM micrographs of high resolution (Figure 4) for the nanolayer electrodeposited in $1.1 \, M \, H_3PO_4$ solution at a current density of $12 \, mA/cm^2$ for 50 min presented a porous microstructure with fine porosity and pore diameter
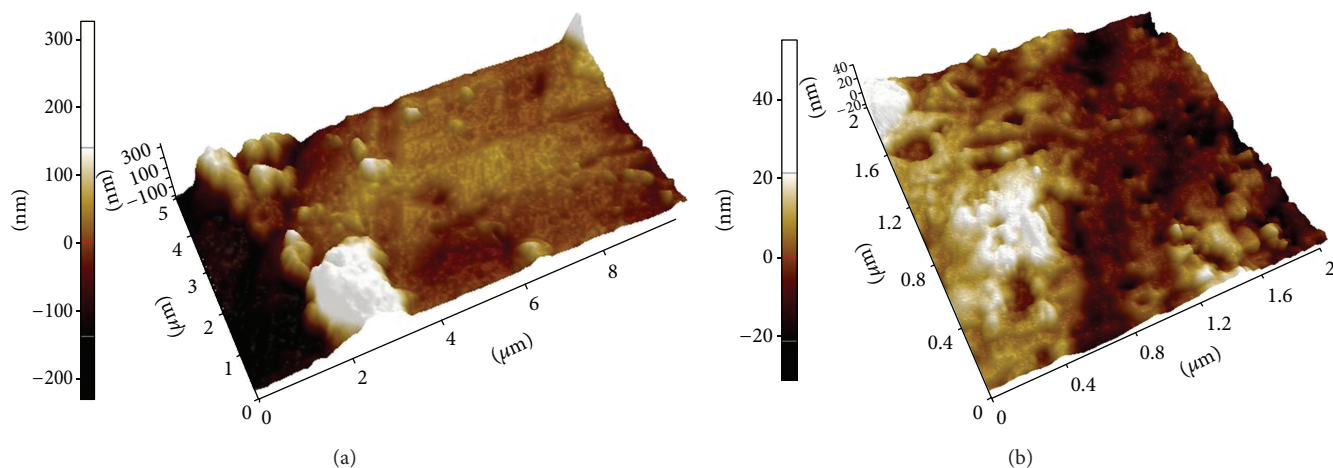
(a)

(b)

FIGURE 3: AFM 3D images for the electrodeposited nanolayers in (a) 0.5 M H_3PO_4, 10 mA/cm^2, 45 min; (b) 1.1 M H_3PO_4, 12 mA/cm^2, 50 min.

FIGURE 4: SEM micrograph for the nanolayer electrodeposited at 12 mA/cm^2, in 1.1 M H_3PO_4 solution for 50 min.

of 20–50 nm. It was shown by Park et al. [38] that a diameter less than 30 nm provided an accelerated cell adhesion and spreading. Also, the nanoporous oxide layer can stimulate the growth of the bone tissue through them, leading to an anchorage, effective fusion with the bone [8, 12, 13]. Therefore, the pore dimensions of our obtained nanolayer are very suitable for an implant material.

XPS, AFM, and SEM analysis demonstrated that the electrodeposited film on the new Ti-15Ta-5Zr alloy surface by the anodic galvanostatic polarization at a current density of 12 mA/cm^2 for 50 min in 1.1 M H_3PO_4 solution was a phosphorous-enriched oxide nanolayer with very good roughness and porosity, that is able to increase the alloy bioactivity, to stimulate the cell growth, and to favor the osseointegration.

3.4. Electrochemical and Corrosion Stability of the Electrodeposited Nanolayer.

The flat potentiodynamic polarization curves (Figure 5) of the bare and anodic oxidized Ti-15Ta-5Zr

alloy in Ringer solutions of different pH values showed a passive behavior.

The corrosion, E_{corr}, and passivation, E_p, potentials (Table 2) for the anodic oxidized alloy shifted towards positive region in comparison with those of the bare alloy, evincing a nobler surface; this fact can be explained by the thicker oxide layer and by its composition enriched with phosphorous ions which inhibits the dissolution processes at the interface and leads to the ennoblement of E_{corr} and E_p [14–16]. Also, the passive current density, i_p, had lower values for the anodic oxidized alloy in comparison with the bare substrate proving that the electrodeposited nanolayer acts as an effective barrier against the aggressive ion entrance through it [7, 8]. The large current plateau is indicative of the unique ion transfer reaction that conducts to the thickening of the oxide nanolayer according to the high field mechanism [7, 11, 39]. Tendency to passivation $|E_{corr} - E_p|$ had lower values for the oxidized alloy as result of the strong passivation action exercised by the electrodeposited nanolayer. The noblest electrochemical behavior, the most favorable electrochemical parameters were registered for the
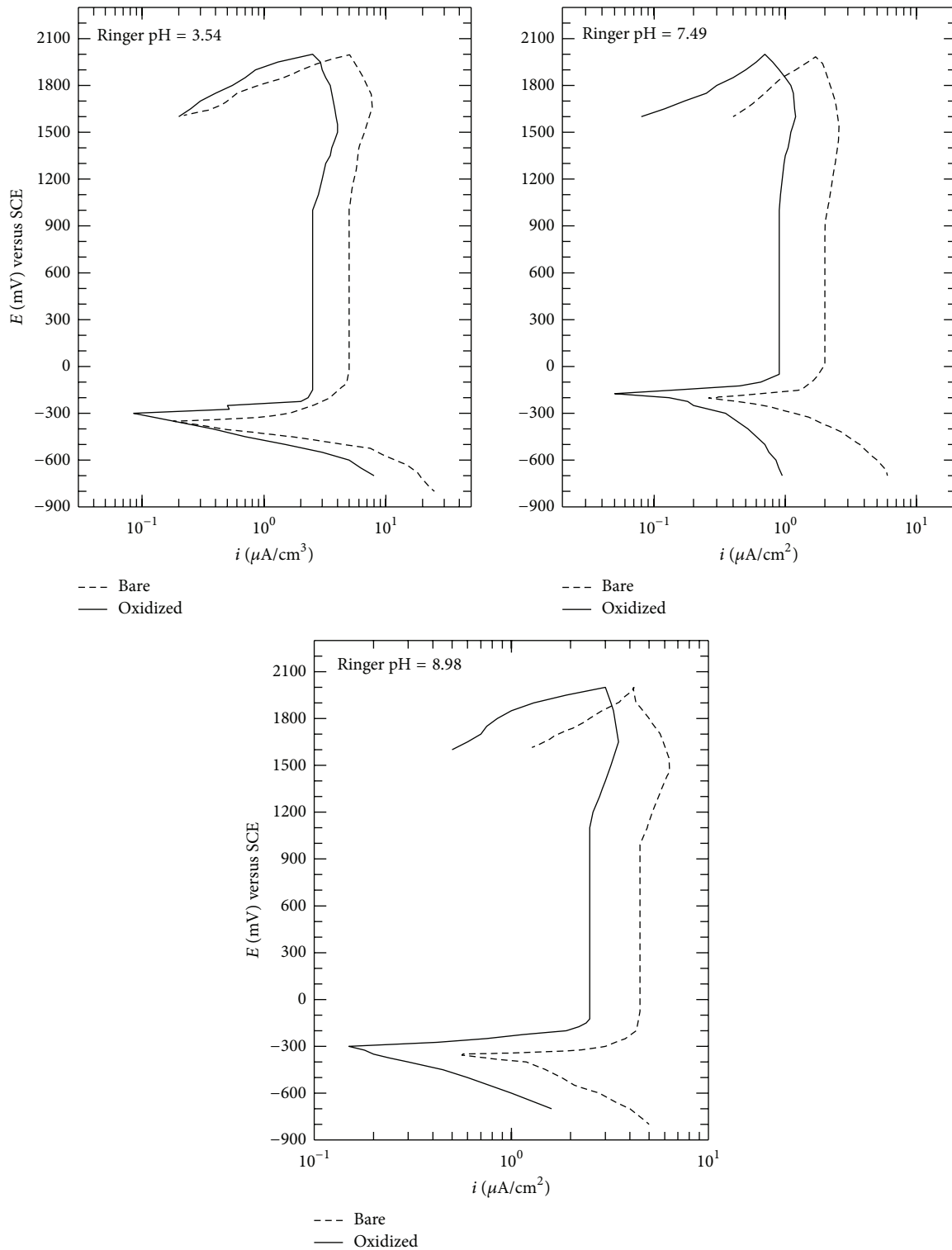
Figure 5: Cyclic potentiodynamic polarization curves for bare and anodic oxidized Ti-15Ta-5Zr alloy in Ringer solutions at 37°C.

oxidized alloy in neutral Ringer solution, the condition in which an implant "works" the longest time period. In acid and alkaline Ringer solutions, slightly unfavorable electrochemical parameters were obtained, but their values demonstrate a passive, resistant state.

The potentiodynamic linear polarization curves, Tafel representation (an example is presented in Figure 6) furnished the main corrosion parameters. The alloy corrosion is very important factor because by corrosion can be released ions and corrosion products which may affect surrounding

TABLE 2: Main electrochemical parameters for bare and anodic oxidized Ti-15Ta-5Zr alloy in Ringer solutions at 37°C.

Parameter	Ringer pH = 3.54		Ringer pH = 7.49		Ringer pH = 8.98	
	Bare	Oxidized	Bare	Oxidized	Bare	Oxidized
E_{corr} (mV)	−350	−300	−200	−150	−350	−300
E_p (mV)	−150	−150	−100	−75	−200	−175
ΔE_p (mV)	>2000	>2000	>2000	>2000	>2000	>2000
$\lvert E_{corr} - E_p \rvert$ (mV)	200	150	100	75	150	125
i_p (μA/cm^2)	5.0	2.5	2.0	0.9	4.5	2.5

TABLE 3: Main corrosion parameters for bare and anodic oxidized Ti-15Ta-5Zr alloy in Ringer solutions at 37°C.

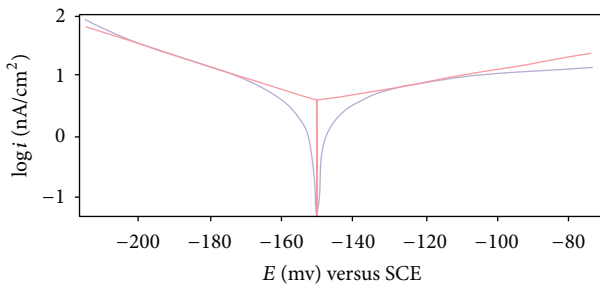| Parameter	Ringer pH = 3.54		Ringer pH = 7.49		Ringer pH = 8.98	
	Bare	Oxidized	Bare	Oxidized	Bare	Oxidized
i_{corr} (μA/cm^2)	0.091	0.019	0.010	0.0053	0.061	0.032
V_{corr} (μm/Year)	0.83	0.171	0.092	0.049	0.556	0.294
R_p (k$\Omega \cdot$cm^2)	184	979	180	1879	133	945
Ion release (ng/cm^2)	84.33	17.37	9.35	4.98	56.49	29.91
Resistance class	PS	PS	PS	PS	PS	PS

PS: perfect stable.

FIGURE 6: Tafel representation for anodic oxidized Ti-15Ta-5Zr alloy in Ringer solution of pH = 7.49 at 37°C.

tissues and may cause inflammatory processes. Applying the anodic galvanostatic oxidation, a thicker nanolayer was formed on the alloy surface that improved all corrosion parameters.

From Table 3 it results in the pronounced decrease (about 7 times) for the values of i_{corr}, and V_{corr}; also, the total quantity of ions released into physiological Ringer solutions decreased very much; namely, the toxicity of the anodic oxidized alloy is much lower than that of the bare one. Comparing with the results of other authors, it appears that our electrodeposited nanolayer confers superior protection to its substrate: Narayanan and Seshadri [16] determined i_{corr} of 0.011 μA/cm^2 in neutral Ringer solution for Ti-6Al-4V alloy covered with a layer of 280 nm thickness; our i_{corr} is 0.0053 μA/cm^2; Simka [8] obtained i_{corr} = 0.010 μA/cm^2 for Ti-13Nb-13Zr alloy anodized at 80 V, thickness of 5–10 nm; Jakubowicz et al. [9] realized i_{corr} = 12.5 μA/cm^2 for Ti-6Zr-4Nb alloy anodic oxidized at 10 V. Polarization resistance, R_p, increased of about 5–10 times in comparison with the bare alloy; that is, the electrodeposited nanolayer put up a much higher resistance to the ion migration through it from metal

to solution and inversely [8]. A R_p value of 1.879 M$\Omega \cdot$cm^2 in neutral Ringer solution is higher than that of 1.160 M$\Omega \cdot$cm^2 measured by Simka [8] for Ti-13Nb-13Zr alloy. The best values for the corrosion parameters were found in neutral Ringer solution, characterizing a "Perfect Stable" resistance class both for bare and oxidized Ti-15Ta-5Zr alloy. Though in acid and alkaline Ringer solutions, less unfavorable parameters were registered, and the two alloys are very resistant, being placed in the same "Perfect Stable" class. Therefore, the electrodeposited nanolayer can protect the alloy from the ion release, minimizing the adverse reactions and increasing its biocompatibility.

Nyquist spectra [15] (Figure 7) recorded in Ringer solutions evinced larger semicircles with bigger radii and higher impedance values for the oxidized alloy in comparison with the bare one; these facts show a capacitive behavior, a film with dielectric properties and that the electrodeposited nanolayer has more insulating, more protective properties and is thicker than that on the bare alloy surface, as was proved by XPS analysis. Also, the best capacitive behavior, the most resistant nanolayer resulted in neutral Ringer solution. Some inflexions can be observed on Nyquist spectra, which denote inhomogeneous films consisting from two or more layers [8, 40].

Bode phase angle plots [11, 13, 14, 19] (Figure 8) revealed in the low and middle frequency range two phase angles with very high values (between −79° and −86°) describing the same capacitive behavior. The anodic oxidized alloy had higher phase angles, with 2°-3° higher than those of the bare one; these phase angles had values of −85° ÷ −86° which indicate a protective film with more insulating properties conferred by the thicker electrodeposited nanolayer [11, 19]; the higher phase angles show a more capacitive, compact, denser, barrier layer (in contact with the metallic substrate), and very resistant to the crossing of the ions through it. The lower phase angles of about −79° ÷ −82° suggest a more
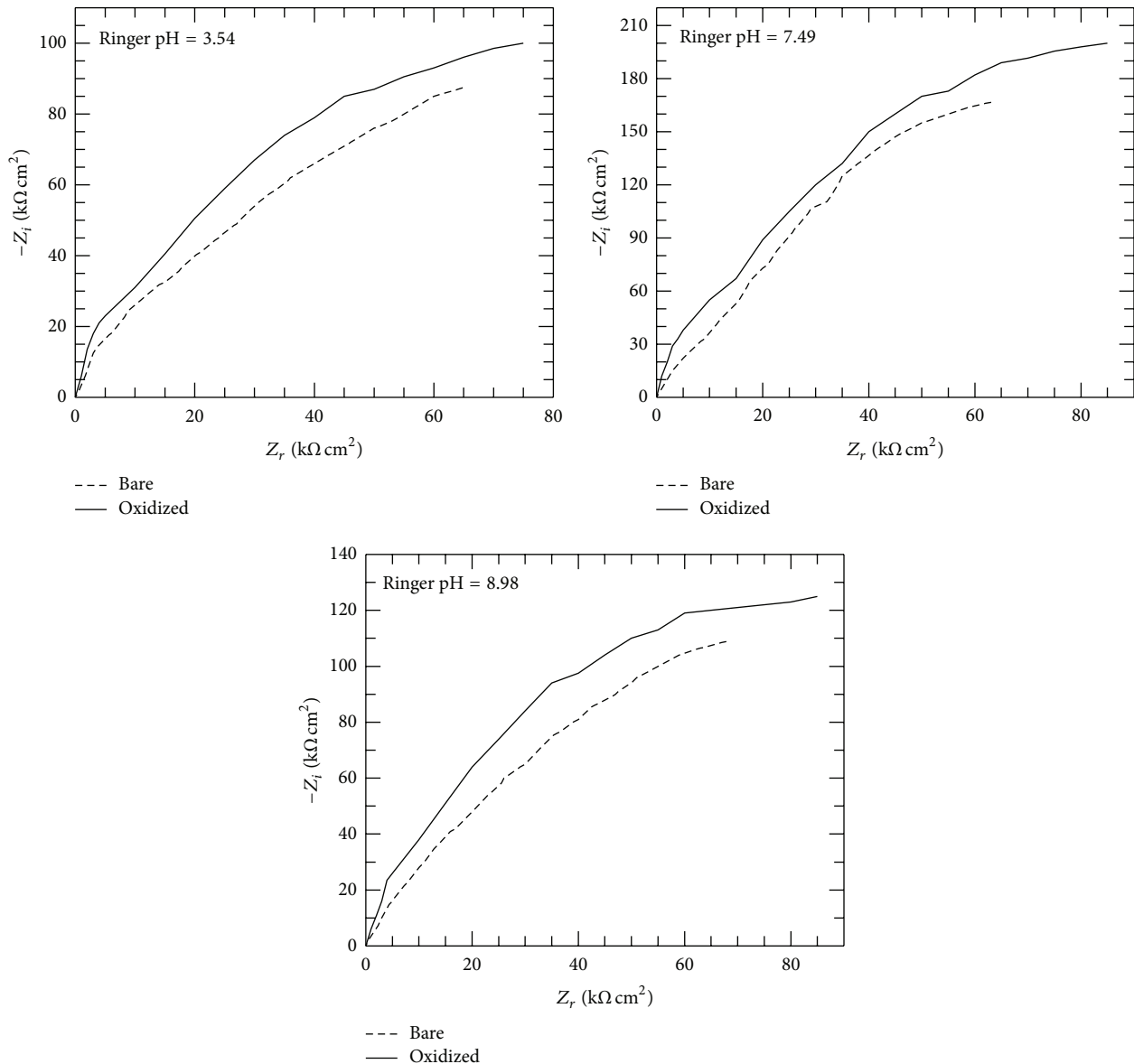
FIGURE 7: Nyquist spectra for bare and anodic oxidized Ti-15Ta-5Zr alloy in Ringer solutions at 37°C.

permissive, porous layer (in contact with the electrolyte) that permits the absorption of the different ions, compounds, and species from solution into its pores [13, 14, 41]; these pores can stimulate the adsorption and growth of the osteoblast cells through them, producing their strong binding [13]. The thicker, denser, more compact electrodeposited nanolayer that contains both protective Ti, Ta, and Zr oxides and PO_4^{3-} ions (XPS data) can reduce the potential gradient across the metal/nanolayer/solution interface, thus reducing the anodic dissolution.

EIS spectra were modeled with two time constant equivalent electric circuit (Figure 9). Many authors [11, 13, 14] used this equivalent circuit to describe the bilayered structure of the surface films grown by the electrochemical anodization. The fitted electric equivalent circuit reflects the barrier properties of the inner, dense, compact layer by its resistance, R_1,

and capacitance, CPE_1, and those of porosity of the outer, less protective porous layer by its resistance, R_2, and capacitance, CPE_2 (instead of capacitance, Q was used constant phase element, CPE that represents a nonideal capacitance).

The impedance parameters from Table 4 showed that the inner, barrier layer resistance, R_1, is higher of two orders of magnitude than that of the porous layer, R_2, demonstrating a very resistive, protective, inner layer [19]; the lower inner layer capacitance, CPE_1, than that of the porous one, CPE_2, can be related to the thickening of this barrier layer [14]. The higher values of n1 parameter between 0.96 and 0.99 in comparison with those of n2 parameter of 0.91–0.93 indicate that the inner barrier layer closed to an ideal capacitor, being the layer that confers real protection to the substrate [11, 19]. All impedance parameters had more favorable values for the anodic oxidized Ti-15Ta-5Zr alloy comparing with the bare
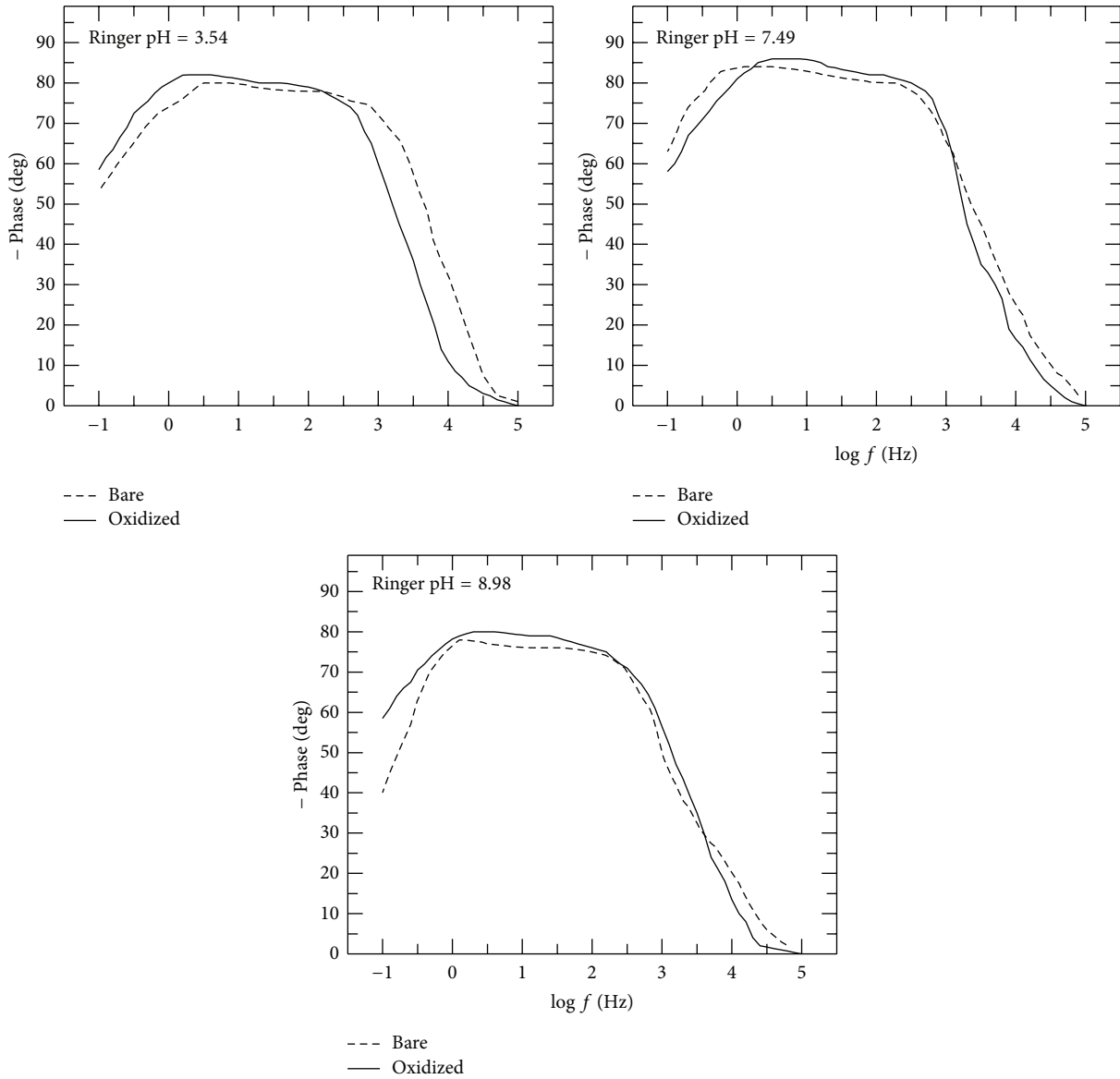
FIGURE 8: Bode spectra for bare and anodic oxidized Ti-15Ta-5Zr alloy in Ringer solutions at 37°C.
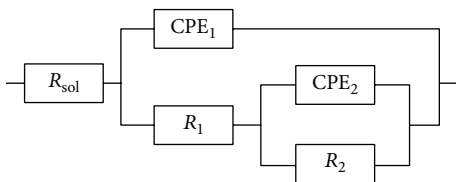

FIGURE 9: Electric equivalent circuit with two time constants.

one, due to the thicker, denser, more compact electrodeposited nanolayer that contains, in addition, protective and bioactive phosphate ions.

3.5. Long-Term Behavior of the Electrodeposited Nanolayer. The long-term behavior (500 immersion hours) of the bare

and anodic oxidized Ti-15Ta-5Zr alloy was studied by the monitoring of the open circuit potentials, E_{oc}, and corresponding open circuit potential gradients, ΔE_{oc}.

E_{oc} (Figure 10) increased over time with almost 100 mV to more positive values; such behavior indicates the thickening [42, 43] of the native passive film for the bare alloy and of the electrodeposited nanolayer for the oxidized alloy, namely, a certain activity into the physiological solutions [8, 13]. The fact that the E_{oc} values for the oxidized alloy are nobler than those for the bare alloy can be explained taking into consideration the higher thickness and the more favorable composition containing incorporated, protective phosphate ions of the electrodeposited nanolayer which lead to the ennoblement of its open circuit potentials [8, 12]. The open circuit potentials reached almost constant values after about 250 immersion hours, proving a resistant, stable state. The most

TABLE 4: Impedance parameters for bare and anodic oxidized Ti-15Ta-5Zr alloy in Ringer solutions at 37°C.

Parameter	Ringer pH = 3.54		Ringer pH = 7.49		Ringer pH = 8.98	
	Bare	Oxidized	Bare	Oxidized	Bare	Oxidized
R_{sol} ($\Omega \cdot cm^2$)	13.2	13.9	14.1	14.7	13.4	13.9
R_1 ($\Omega \cdot cm^2$)	7.9×10^6	8.5×10^6	8.7×10^6	9.9×10^6	7.5×10^6	8.3×10^6
CPE_1 ($S \cdot s^n/cm^2$)	2.7×10^{-6}	1.7×10^{-6}	3.1×10^{-6}	1.5×10^{-6}	2.4×10^{-5}	1.9×10^{-5}
$n1$	0.97	0.98	0.98	0.99	0.96	0.97
R_2 ($\Omega \cdot cm^2$)	1.6×10^4	1.8×10^4	2.1×10^4	2.5×10^4	1.8×10^4	2.1×10^4
CPE_2 ($S \cdot s^n/cm^2$)	1.5×10^{-5}	1.2×10^{-5}	1.1×10^{-5}	1.0×10^{-5}	1.4×10^{-5}	1.2×10^{-5}
$n2$	0.91	0.92	0.92	0.93	0.91	0.92
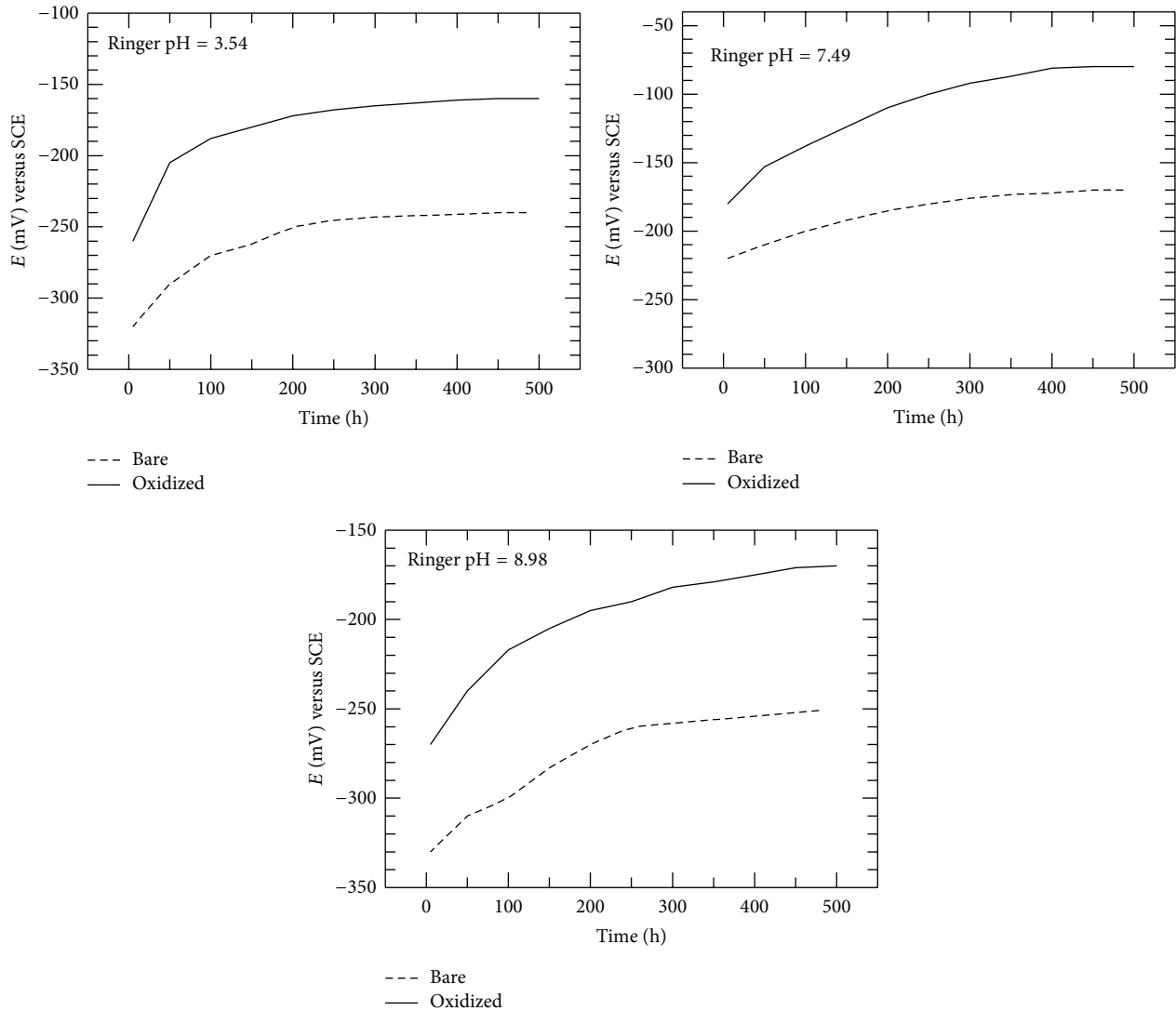
FIGURE 10: E_{oc} versus time for bare and anodic oxidized Ti-15Ta-5Zr alloy in Ringer solutions at 37°C.

electropositive values of E_{oc} were registered in neutral Ringer solution, that is, the most protective, resistant behavior.

The open circuit potential gradients, ΔE_{oc} (pH), which can appear along the implant surface, due to the local pH nonuniformity of the physiological fluid are presented in Table 5; very low values were obtained; these gradient values cannot initiate galvanic cells or local corrosion, because, as was shown by many authors [35, 36, 44], only potential differences of 0.6-0.7 V can develop these kinds of corrosion. Therefore, both bare and anodic oxidized Ti-15Ta-5Zr alloy

Table 5: Open circuit potential gradients versus time for bare and anodic oxidized Ti-15Ta-5Zr alloy in Ringer solutions at 37°C.

Ti-15Ta-5Zr	Time	ΔE_{oc1} (mV)	ΔE_{oc2} (mV)	ΔE_{oc3} (mV)
Bare	0	−70	−67	3
	200	−35	−18	17
	500	−31	−28	30
Oxidized	0	−80	10	110
	200	−62	23	85
	500	−80	10	90

have no susceptibility to galvanic or local corrosion for long term (500 exposure hours till present) even in severe functional conditions of extreme pH values.

It showed that the electrodeposited nanolayer can assure long-term corrosion resistance.

4. Conclusions

XPS, AFM, and SEM analysis demonstrated that the electrodeposited film on the new Ti-15Ta-5Zr alloy surface, by the anodic galvanostatic polarization at a current density of $12\,\mathrm{mA/cm^2}$ for 50 min in 1.1 M H_3PO_4 solution was a phosphorous-enriched oxide nanolayer with very good roughness and porosity, proper microstructure, composition and thickness. All electrochemical parameters for the oxidized alloy had more favorable values than those of the bare alloy, indicative of the strong passivation action exercised by the electrodeposited nanolayer. The anodic oxidation nanolayer improved all corrosion parameters conferring superior protection to the Ti-15Ta-5Zr alloy substrate by its higher resistance to the ion migration through it. Impedance spectra revealed that the electrodeposited nanolayer has more insulating, protective properties and is thicker (as was proved by XPS determinations) in comparison with the native film on the bare alloy surface. The electrodeposited nanolayer is formed by an inner, compact, dense, barrier layer, very resistant to the crossing of the ions through it, and an outer, more permissive, porous layer that permits the absorption of the different species, stimulating the growth and strong binding of the bone cells. The open circuit potentials increased over time with almost 100 mV to more positive values; such behavior indicates the thickening of the electrodeposited nanolayer, namely, its bioactivity. The oxidized nanolayer is able to protect the alloy from ion release, to assure long-term corrosion resistance, to minimize adverse reactions, to increase the alloy bioactivity, to stimulate the cell growth, and to favor the osseointegration.

Conflict of Interests

The authors declare that there is no conflict of interests regarding the publication of this paper.
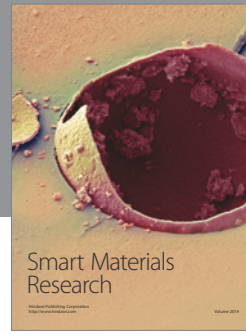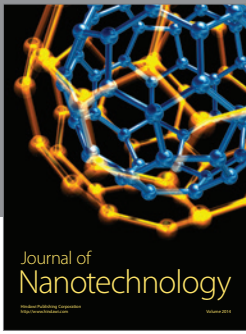
References

[1] Z. Li, C. Ning, D. Ding, H. Liu, and L. Huang, "Biological properties of Ti-Nb-Zr-O nanostructures grown on Ti35Nb5Zr alloy," *Journal of Nanomaterials*, vol. 2012, Article ID 834042, 7 pages, 2012.

[2] P. K. Zysset, X. E. Guo, C. E. Hoffler, K. E. Moore, and S. A. Goldstein, "Mechanical properties of human trabecular bone lamellae quantified by nanoindentation," *Technology and Health Care*, vol. 6, no. 5-6, pp. 429–432, 1998.

[3] M. Niinomi, "Recent research and development in titanium alloys for biomedical applications and healthcare goods," *Science and Technology of Advanced Materials*, vol. 4, no. 5, pp. 445–454, 2003.

[4] V. S. Saji and H. C. Choe, "Electrochemical corrosion behaviour of nanotubular Ti-13Nb-13Zr alloy in Ringer's solution," *Corrosion Science*, vol. 51, no. 8, pp. 1658–1663, 2009.

[5] C.-K. Lee, "Fabrication, characterization and wear corrosion testing of bioactive hydroxyapatite/nano-TiO_2 composite coatings on anodic Ti-6Al-4V substrate for biomedical applications," *Materials Science and Engineering B*, vol. 177, no. 11, pp. 810–818, 2012.

[6] E. Peláez-Abellán, L. Rocha-Sousa, W.-D. Müller, and A. C. Guastaldi, "Electrochemical stability of anodic titanium oxide films grown at potentials higher than 3 V in a simulated physiological solution," *Corrosion Science*, vol. 49, no. 3, pp. 1645–1655, 2007.

[7] M. P. Neupane, I. S. Park, S. J. Lee, K. A. Kim, M. H. Lee, and T. S. Bae, "Study of anodic oxide films of titanium fabricated by voltammetric technique in phosphate buffer media," *International Journal of Electrochemical Science*, vol. 4, no. 2, pp. 197–207, 2009.

[8] W. Simka, "Preliminary investigations on the anodic oxidation of Ti-13Nb-13Zr alloy in a solution containing calcium and phosphorus," *Electrochimica Acta*, vol. 56, no. 27, pp. 9831–9837, 2011.

[9] J. Jakubowicz, G. Adamek, M. U. Jurczyk, and M. Jurczyk, "3D surface topography study of the biofunctionalised nanocrystalline Ti-6Zr-4Nb/Ca-P," *Materials Characterization*, vol. 70, pp. 55–62, 2012.

[10] M. V. Popa, E. Vasilescu, P. Drob et al., "Corrosion resistance improvement of titanium base alloys," *Quimica Nova*, vol. 33, no. 9, pp. 1892–1896, 2010.

[11] M. T. Woldemedhin, D. Raabe, and A. W. Hassel, "Characterization of thin anodic oxides of Ti-Nb alloys by electrochemical impedance spectroscopy," *Electrochimica Acta*, vol. 82, pp. 324–332, 2012.

[12] S.-E. Kim, S.-B. Lee, S.-W. Kwak, C.-K. Kim, and K. N. Kim, "Nanoporous anodic oxidation titanium enhances cell proliferation and differentiation of immortalized mouse embryonic cells," *Surface & Coatings Technology*, vol. 228, supplement 1, pp. S37–S42, 2013.

[13] L. T. Duarte, S. R. Biaggio, R. C. Rocha-Filho, and N. Bocchi, "Surface characterization of oxides grown on the Ti-13Nb-13Zr

alloy and their corrosion protection," *Corrosion Science*, vol. 72, pp. 35–40, 2013.

[14] A. Gomez Sanchez, J. Ballarre, J. C. Orellano, G. Duffo, and S. Cere, "Surface modification of zirconium by anodisation as material for permanent implants: in vitro and in vivo study," *Journal of Materials Science: Materials in Medicine*, vol. 24, no. 1, pp. 161–169, 2013.

[15] R. Narayanan and S. K. Seshadri, "Phosphoric acid anodization of Ti-6Al-4V—structural and corrosion aspects," *Corrosion Science*, vol. 49, no. 2, pp. 542–558, 2007.

[16] R. Narayanan and S. K. Seshadri, "Point defect model and corrosion of anodic oxide coatings on Ti-6Al-4V," *Corrosion Science*, vol. 50, no. 6, pp. 1521–1529, 2008.

[17] Y. Shibata, D. Suzuki, S. Omori et al., "The characteristics of in vitro biological activity of titanium surfaces anodically oxidized in chloride solutions," *Biomaterials*, vol. 31, no. 33, pp. 8546–8555, 2010.

[18] H. Habazaki, M. Teraoka, Y. Aoki, P. Skeldon, and G. E. Thompson, "Formation of porous anodic titanium oxide films in hot phosphate/glycerol electrolyte," *Electrochimica Acta*, vol. 55, no. 12, pp. 3939–3943, 2010.

[19] S. K. Poznyak, A. D. Lisenkov, M. G. S. Ferreira, A. I. Kulak, and M. L. Zheludkevich, "Impedance behaviour of anodic TiO_2 films prepared by galvanostatic anodisation and powerful pulse discharge in electrolyte," *Electrochimica Acta*, vol. 76, pp. 453–461, 2012.

[20] M. V. Popa, I. Demetrescu, E. Vasilescu, P. Drob, D. Ioniţă, and C. Vasilescu, "Stability of some dental implant materials in oral biofluids," *Revue Roumaine de Chimie*, vol. 50, no. 5, pp. 399–406, 2005.

[21] M. V. Popa, E. Vasilescu, P. Drob, and C. Vasilescu, "The modeling of passive film formation on a new industrial titanium alloy in very aggressive environment," *Revista de Chimie*, vol. 56, no. 9, pp. 908–912, 2005.

[22] E. Vasilescu, P. Drob, C. Vasilescu et al., "Corrosion resistance of the new Ti-25Ta-25Nb alloy in severe functional conditions," *Materials and Corrosion*, vol. 61, no. 11, pp. 947–954, 2010.

[23] M. V. Popa, J. M. C. Moreno, M. Popa et al., "Electrochemical deposition of bioactive coatings on Ti and Ti-6Al-4V surfaces," *Surface and Coatings Technology*, vol. 205, no. 20, pp. 4776–4783, 2011.

[24] D. Portan, D. Ionita, and I. Demetrescu, "Monitoring TiO_2 nanotubes elaboration condition, a way for obtaining various characteristics of nanostructures," *Key Engineering Materials*, vol. 415, pp. 9–12, 2009.

[25] M. Mîndroiu, C. Pirvu, R. Ion, and I. Demetrescu, "Comparing performance of nanoarchitectures fabricated by Ti6Al7Nb anodizing in two kinds of electrolytes," *Electrochimica Acta*, vol. 56, no. 1, pp. 193–202, 2010.

[26] M. Prodana, D. Ionita, C. Ungureanu, D. Bojin, and I. Demetrescu, "Enhancing antibacterial effect of multiwalled carbon nanotubes using silver nanoparticles," *Digest Journal of Nanomaterials and Biostructures*, vol. 6, no. 2, pp. 549–556, 2011.

[27] E. Vasilescu, P. Drob, D. Raducanu et al., "Effect of thermomechanical processing on the corrosion resistance of Ti6Al4V alloys in biofluids," *Corrosion Science*, vol. 51, no. 12, pp. 2885–2896, 2009.

[28] M. A. Baker, S. L. Assis, R. Grilli, and I. Costa, "Investigation of the electrochemical behaviour and surface chemistry of a Ti-13Nb-13Zr alloy exposed in MEM cell culture media with and without the addition of H_2O_2," *Surface and Interface Analysis*, vol. 40, no. 3-4, pp. 220–224, 2008.

[29] R. Van Noort, "Titanium: the implant material of today," *Journal of Materials Science*, vol. 22, no. 11, pp. 3801–3811, 1987.

[30] J. F. Moulder, W. F. Stickle, P. E. Sobol, and K. D. Bomben, *Handbook of X-Ray Photoelectron Spectroscopy*, Physical Electronics, Chamhassen, Minn, USA, 1995.

[31] A. V. Naumkin, A. Kraut-Vass, S. W. Gaarenstroom, and C. J. Powell, "NIST X-ray photoelectron spectroscopy database," in *NIST Standard Reference Database 20, Version 4.1*, US Secretary of Commerce on behalf of the United States of America, Washington, DC, USA, 2012.

[32] T. Kasuga, M. Nogami, M. Niinomi, and T. Hattori, "Bioactive calcium phosphate invert glass-ceramic coating on β-type Ti-29Nb-13Ta-4.6Zr alloy," *Biomaterials*, vol. 24, no. 2, pp. 283–290, 2003.

[33] S. J. Li, R. Yang, M. Niinomi, Y. L. Hao, and Y. Y. Cui, "Formation and growth of calcium phosphate on the surface of oxidized Ti-29Nb-13Ta-4.6Zr alloy," *Biomaterials*, vol. 25, no. 13, pp. 2525–2532, 2004.

[34] I. S. Park, U. J. Choi, H. K. Yi, B. K. Park, M. H. Lee, and T. S. Baea, "Biomimetic apatite formation and biocompatibility on chemically treated Ti-6Al-7Nb alloy," *Surface and Interface Analysis*, vol. 40, no. 1, pp. 37–42, 2008.

[35] G. Sheela, M. Ramasamy, C. R. K. Rao, and M. Pushpavanam, "Electrochemical assessment on corrosion behaviour of electrochemically joined dissimilar metal joints," *Bulletin of Electrochemistry*, vol. 17, no. 8, pp. 347–350, 2001.

[36] E. Blasco-Tamarit, A. Igual-Muñoz, J. G. Antón, and D. M. García-García, "Galvanic corrosion of titanium coupled to welded titanium in LiBr solutions at different temperatures," *Corrosion Science*, vol. 51, no. 5, pp. 1095–1102, 2009.

[37] D. R. Baer, M. H. Engelhard, A. S. Lea et al., "Comparison of the sputter rates of oxide films relative to the sputter rate of SiO2," *Journal of Vacuum Science and Technology A: Vacuum, Surfaces and Films*, vol. 28, no. 5, pp. 1060–1072, 2010.

[38] J. Park, S. Bauer, K. Von Der Mark, and P. Schmuki, "Nanosize and vitality: TiO_2 nanotube diameter directs cell fate," *Nano Letters*, vol. 7, no. 6, pp. 1686–1691, 2007.

[39] M. M. Lohrengel, "Thin anodic oxide layers on aluminium and other valve metals: high field regime," *Materials Science and Engineering R: Reports*, vol. 11, no. 6, pp. 243–294, 1993.

[40] S. L. Assis and I. Costa, "Electrochemical evaluation of Ti-13Nb-13Zr, Ti-6Al-4V and Ti-6Al-7Nb alloys for biomedical application by long-term immersion tests," *Materials and Corrosion*, vol. 58, no. 5, pp. 329–333, 2007.

[41] S. Tamilselvi and N. Rajendran, "In vitro corrosion behaviour of Ti-5Al-2Nb-1Ta alloy in Hanks solution," *Materials and Corrosion*, vol. 58, no. 4, pp. 285–289, 2007.

[42] J. Black, *Biological Performance of Materials: Fundamentals of Biocompatibility*, Marcel Dekker, New York, NY, USA, 1992.

[43] D. J. Blackwood, A. W. C. Chua, K. H. W. Seah, R. Thampuran, and S. H. Teoh, "Corrosion behaviour of porous titanium-graphite composites designed for surgical implants," *Corrosion Science*, vol. 42, no. 3, pp. 481–503, 2000.

[44] Q. K. Guo, M. Du, and C. J. Zhou, "Study of galvanic corrosion of carbon steel/titanium and carbon steel/titanium/navel brass in seawater," in *Proceedings of the 16th International Corrosion Congress*, paper 08-28, pp. 08–28, Beijing, China, September 2005.

Journal of
Nanotechnology

International Journal of
Corrosion

International Journal of
Polymer Science

Smart Materials
Research

Journal of
Composites

BioMed
Research International

Journal of
Metallurgy

Journal of
Materials

Hindawi

Submit your manuscripts at
http://www.hindawi.com

Journal of
Nanoparticles

Advances in
Materials Science and Engineering

Scientifica

Journal of
Nanomaterials

The Scientific
World Journal

International Journal of
Biomaterials

Journal of
Nanoscience

Journal of
Coatings

Journal of
Crystallography

Journal of
Ceramics

Journal of
Textiles